International Scientific Conference 20 UNITECH 26

INTERNATIONAL SCIENTIFIC CONFERENCE
19-21 November 2026
GABROVO

KINEMATIC MODELING AND MOBILITY ASSESSMENT OF FOUR-TRACK SKID-STEERED MOBILE ROBOTS FOR SEARCH-AND-RESCUE APPLICATIONS

Yanko Boyanov, Orlin Petrov, Tsvetelina Georgieva

"Angel Kanchev" University of Ruse, 8 Studentska str., Ruse, Bulgaria

……

**Corresponding author: yboyanov@uni-ruse.bg*

Abstract

Tracked unmanned ground vehicles (UGVs) are widely used in search-and-rescue applications because of their extended ground contact and skid-steering capabilities, which support mobility on irregular terrain and in confined environments. Among these systems, rigid four-track architectures offer a potential compromise between the structurally simple, conventional dual-track vehicles and the greater terrain adaptability, but higher mechanical complexity of articulated tracked robots. This study develops a generalized planar kinematic model for a rigid four-track skid-steered UGV and examines its mobility characteristics relevant to search-and-rescue operations. The methodological steps include a geometric representation of four independently driven track modules, derivation of forward and inverse kinematics, formulation of a 2x4 equivalent Jacobian matrix, analytical assessment of turning behavior, contact area, nominal ground pressure, and obstacle-negotiation characteristics. The model shows that the four actuator velocities map to two body-motion variables—longitudinal velocity and yaw rate, while the longitudinal spacing between the front and rear modules does not enter the reduced Jacobian under symmetric rigid-body assumptions. The proposed framework provides a compact basis for control, odometry and mobility analysis of rigid four-track skid-steered UGVs and clarifies their advantages and limitations for search-and-rescue applications.

Keywords: four-tracked robot, kinematic model, mobility assessment, search and rescue.

INTRODUCTION

Search-and-rescue (SAR) robots are expected to enter environments in which direct human intervention is dangerous, delayed, or impossible. Collapsed buildings, damaged industrial facilities, rubble, loose soil, stairs, and confined passages impose simultaneous requirements for mobility, robustness, sensing, and reliable teleoperation or autonomy [1,2]. The locomotion mechanism is therefore a primary design decision. Previous studies of urban SAR platforms show that wheeled, tracked, legged, and hybrid systems offer different strengths and limitations. Their suitability depends on the terrain, access constraints, and mission requirements. Therefore, no single architecture is optimal for all disaster scenarios [3].

Tracked locomotion is attractive for SAR applications because it distributes vehicle weight and tractive effort over a relatively large contact area. This extended contact with the ground affects how the vehicle interacts with the terrain. Ground-vehicle theory relates this interaction to sinkage, traction, and motion resistance [4]. Compact tracked robots commonly use skid steering. The vehicle turns by driving the left and right tracks at different longitudinal speeds, without a separate steering linkage. This enables a small nominal turning radius, including an ideal zero-radius turn, but it also requires lateral relative motion at the

This is an open access article licensed under Creative Commons Attribution 4.0 International
Print ISSN: 1313-230X, Online ISSN: 3033-1404

track-ground interface. Experimental and analytical studies show that the resulting skid shifts the instantaneous center of rotation, degrades odometric accuracy, and increases steering losses [5,6].

Rigid four-track skid-steered UGVs use separate front and rear tracked modules on each side [7]. Other tracked robots adapt to terrain in different ways. Passive suspension can improve contact continuity on uneven terrain, although it introduces additional degrees of freedom and increases mechanical complexity [8,9]. Articulated robots with flippers take a more active approach. They change their configuration to negotiate stairs, stepfields, and other severe obstacles. This adaptability requires additional joints and actuators and makes both the mechanical design and the control system more complex [10,11].

These alternatives allow the architectures to be compared in terms of terrain adaptability, mechanical complexity, and modeling requirements without implying that one is universally superior.

The problem addressed in this paper is the need for a compact, platform-independent formulation that explicitly retains four tracked actuators while separating the geometry that governs nominal planar motion from the geometry that governs contact distribution and obstacle negotiation. The aim of the study is to derive such a model for symmetric rigid four-track skid-steered UGVs. The principal limitation is that the model is kinematic: track-terrain deformation, longitudinal slip, lateral skid, motor dynamics, load transfer, and body pitch and roll are not predicted. Accordingly, the equations define a nominal control and odometry model rather than a complete terramechanical description.

The resulting formulation is used to examine the mobility characteristics of the architecture in the context of search-and-rescue applications. It also provides a common basis for discussing turning behavior, ground contact, and obstacle negotiation within the same geometric framework. This enables a direct comparison between the rigid four-track arrangement and other representative tracked UGV architectures.

EXPOSITION

The study has four objectives:

- define a generalized geometry for four separated tracked propulsion modules;
- derive forward and inverse kinematics together with an equivalent four-track Jacobian matrix;
- identify analytical mobility indicators relevant to SAR;
- compare the principal advantages and disadvantages of representative tracked UGV architectures.

The working hypothesis is that a rigid four-track configuration occupies a useful middle ground between mechanically simple dual-track platforms and highly reconfigurable articulated robots. It keeps the chassis rigid and avoids the additional joints used in articulated systems. At the same time, the separated front and rear track modules provide a more distributed contact arrangement than a conventional dual-track layout. This configuration is expected to be most useful when robust construction, compact maneuvering, modular propulsion, and a stable payload platform are more important than extreme obstacle negotiation capability.

Tracked robot architectures differ in how they maintain ground contact and adapt to obstacles. Conventional rigid tracks, passive suspension, and articulated flippers address this problem in different ways. The rigid four-track arrangement considered in this study represents another approach, in which the contact region is divided between separate front and rear propulsion modules. Table 1 summarizes the main advantages and limitations of these architectures. It shows that no single architecture is suitable for every type of terrain. Rigid dual-track robots have relatively simple mechanical layouts, but they cannot actively adapt their support geometry to obstacles. Passive suspension allows the running gear to follow

uneven terrain, while articulated flippers can actively change the way the robot approaches stairs and large obstacles. Both approaches improve terrain adaptation, but they also add moving parts or actuators.

Table 1. Comparative characteristics of representative tracked UGV architectures

Architecture	Principal advantages	Principal disadvantages	Sources
Rigid dual-track	Low mechanical complexity; mature skid-steer modeling; compact drivetrain; nominal in-place turning.	Lateral scrubbing and energy loss during turns; terrain conformity depends strongly on track geometry and any suspension.	[3,5,6]
Rigid four-track skid-steer	Four explicit propulsion modules; modular actuation; separated front/rear contact regions; compact skid steering without articulated joints.	More actuators than a two-track drivetrain; rigid module spacing cannot actively conform to large obstacles; skid-steering losses remain.	[7]
Tracked with passive suspension	Passive adaptation to uneven terrain; improved continuity of track-ground contact without commanding every suspension degree of freedom.	Additional joints and moving parts; changing geometry and terrain interaction increase modeling and estimation complexity.	[8,9]
Articulated / flipper tracked	Reconfigurable approach and support geometry; strong capability on stairs, rails, stepfields, and severe obstacles.	Additional actuators, mass, planning variables, and maintenance burden; more complex operator or autonomous control.	[3,10,11]

The rigid four-track arrangement takes a different approach. It divides the propulsion system into separate front and rear modules while keeping the main structure rigid. This avoids the additional joints required by flipper systems, but the fixed distance between the modules limits how the vehicle can adapt to large obstacles. The architecture is therefore most useful when compact skid steering and a mechanically rigid platform are more important than extreme obstacle-climbing capability.

Figure 1 defines the platform-independent geometry and notation used in the derivation. The front direction is the positive body x-axis, the left side is the positive body y-axis, L is the longitudinal spacing between rear and front module centers, and B is the lateral spacing between the left and right module centerlines.

The four modules are denoted FL, FR, RL, and RR according to their position on the vehicle. Their separate representation is important because each module has its own drive input. At the same time, the chassis remains rigid, so the relative positions of the modules do not change during motion

Kinematic Model

Geometry and Assumptions

The model treats the vehicle as a rigid body moving on a locally planar surface. Four identical track modules occupy the front-left (FL), front-right (FR), rear-left (RL), and rear-right (RR) positions shown in Fig. 1. A body-fixed frame is placed at the geometric center. Its x-axis points forward, its y-axis points left, and its z-axis points upward. The main geometric quantities are the lateral spacing B, the longitudinal spacing L, the effective drive radius r_e, the contact length of one module, and the track width.

The model assumes that the chassis remains rigid and that the vehicle moves in a plane. Each track module uses a constant effective drive radius, so its nominal belt speed equals the drive angular speed multiplied by that radius. For the basic inverse solution, the front and rear modules

on the same side receive the same command. This last condition is a control choice rather than a mechanical restriction; the Jacobian still keeps all four actuator inputs.

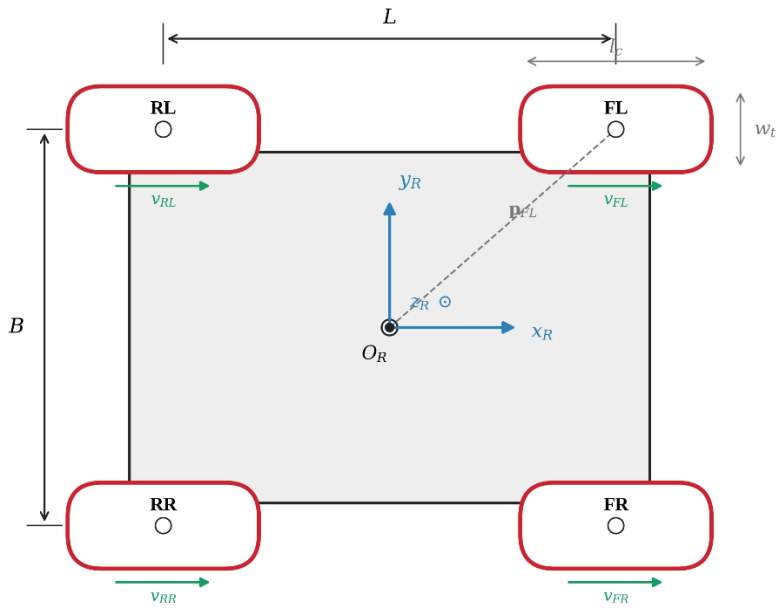


***Fig. 1**. Generalized geometry and notation for a symmetric rigid four-track skid-steered UGV.*

The module-center position vectors, expressed in the body-fixed frame, are:

$$\mathbf{p}_{\mathrm{FL}} = \left[\frac{L}{2}, \frac{B}{2}, 0\right]^{\mathrm{T}} \quad (1)$$

$$\mathbf{p}_{\mathrm{FR}} = \left[\frac{L}{2}, -\frac{B}{2}, 0\right]^{\mathrm{T}} \quad (2)$$

Equations (1) and (2) locate the front-left and front-right module centers in the body frame. L is the distance between the front and rear module centerlines, B is the distance between the left and right centerlines, and the superscript T denotes vector transpose. Distances are expressed in meters.

$$\mathbf{p}_{\mathrm{RL}} = \left[-\frac{L}{2}, \frac{B}{2}, 0\right]^{\mathrm{T}} \quad (3)$$

$$\mathbf{p}_{\mathrm{RR}} = \left[-\frac{L}{2}, -\frac{B}{2}, 0\right]^{\mathrm{T}} \quad (4)$$

Equations (3) and (4) give the same coordinates for the rear-left and rear-right modules. They use the same L and B defined in Eqs. (1) and (2).

Equations (1)-(4) show where L enters the physical geometry. It disappears from the reduced planar velocity equations derived below because the front and rear modules contribute symmetrically. Even so, L still affects how the robot is supported, how loads move between modules, and how the modules meet an obstacle. A model that includes slip, load transfer, or body dynamics would need this geometry explicitly.

Forward Kinematics

For each track module, the drive sprocket produces the nominal longitudinal belt speed

$$v_i = r_e \omega_i \quad (5)$$

Here v_i is the nominal belt speed in meters per second, r_e is the effective drive radius in meters, and ω_i is the drive angular velocity in radians per second. The equation gives the nominal belt speed. During a real skid-steered turn, this speed may differ from the module's ground-relative velocity because of slip.

The front and rear modules on each side are combined into equivalent left- and right-side speeds:

$$v_L = \frac{v_{\mathrm{FL}} + v_{\mathrm{RL}}}{2} \quad (6)$$

$$v_R = \frac{v_{\mathrm{FR}} + v_{\mathrm{RR}}}{2} \quad (7)$$

The two equations simply average the front and rear belt speeds on each side. Both v_L and v_R are measured in meters per second.

The vehicle's nominal forward speed is then:

$$v_x = \frac{r_e}{4}(\omega_{\mathrm{FL}} + \omega_{\mathrm{FR}} + \omega_{\mathrm{RL}} + \omega_{\mathrm{RR}}) \quad (8),$$

where v_x is the longitudinal speed of the vehicle reference point in meters per second. The four angular velocities are the drive speeds of the individual modules, in radians per second, and r_e converts them to belt speed.

The difference between the right- and left-side speeds produces the nominal yaw rate:

With B measured between the left and right module centerlines, the nominal yaw rate is

$$\omega_z = \frac{r_e}{2B}(\omega_{\mathrm{FR}} + \omega_{\mathrm{RR}} - \omega_{\mathrm{FL}} - \omega_{\mathrm{RL}}) \quad (9)$$

A positive value of ω_z corresponds to a left turn under the adopted right-handed coordinate convention. The rate is measured in radians per second.

The planar pose is described by the global position x, y and the heading angle θ. Their rates are:

$$\dot{x} = v_x \cos\theta \quad (10)$$

$$\dot{y} = v_x \sin\theta \quad (11)$$

$$\dot{\theta} = \omega_z \quad (12)$$

where v_x is the body-frame forward speed, and ω_z is the yaw rate from Eq. (9).

Equations (5)-(12) describe the nominal motion of the vehicle. During a real skid-steered turn, the tracks move laterally relative to the ground, and the actual instantaneous center of rotation changes with terrain and operating conditions [5].

Equivalent Four-Track Jacobian Matrix

All four track modules are fixed to the chassis and point in the same longitudinal direction; they do not steer about separate vertical axes. The vehicle turns only because the left and right sides run at different speeds. Let **u** contain the four drive angular velocities in the order FL, FR, RL, RR and let **v** contain the forward speed v_x and yaw rate ω_z. Their nominal relation is

$$\mathbf{v} = \mathbf{J}\mathbf{u} \quad (13)$$

where **J** is the equivalent four-track Jacobian matrix.

For the symmetric rigid geometry, the matrix is

$$\mathbf{J} = \begin{bmatrix} \frac{r_e}{4} & \frac{r_e}{4} & \frac{r_e}{4} & \frac{r_e}{4} \\ -\frac{r_e}{2B} & \frac{r_e}{2B} & -\frac{r_e}{2B} & \frac{r_e}{2B} \end{bmatrix} \quad (14)$$

The first row averages the four drive contributions to forward motion. The second row gives opposite signs to the left and right modules, so their speed difference produces yaw. The longitudinal spacing L does not appear because the front and rear modules on each side contribute symmetrically.

For nonzero r_e and B, the Jacobian has rank two. Four actuator speeds therefore determine only two body motions, leaving two internal actuator degrees of freedom. The model also assumes negligible longitudinal slip and symmetric track-ground interaction. It does not calculate the lateral skid that occurs during a real turn, so the Jacobian should be used as a nominal control and track-based odometry relation rather than as a full terrain model.

Inverse Kinematics

Because **J** has two rows and four columns, it has no conventional inverse. For a desired forward velocity v_x^d and yaw rate ω_z^d, the Moore–Penrose pseudoinverse gives the corresponding drive angular velocities:

$$\mathbf{u}^d = \mathbf{J}^{\dagger}\mathbf{v}^d \quad (15)$$

The pseudoinverse used in Eq. (15) is

$$\mathbf{J}^{\dagger} = \begin{bmatrix} \frac{1}{r_e} & -\frac{B}{2r_e} \\ \frac{1}{r_e} & \frac{B}{2r_e} \\ \frac{1}{r_e} & -\frac{B}{2r_e} \\ \frac{1}{r_e} & \frac{B}{2r_e} \end{bmatrix} \quad (16)$$

The second column gives opposite yaw contributions to the left and right modules. The same r_e and B used in the forward model are retained.

Expanding Eqs. (15) and (16) gives the angular velocity commands for the four drive modules:

$$\omega_{\mathrm{FL}}^{d} = \omega_{\mathrm{RL}}^{d} = \frac{v_x^d - \frac{B}{2}\omega_z^d}{r_e} \quad (17)$$

$$\omega_{\mathrm{FR}}^{d} = \omega_{\mathrm{RR}}^{d} = \frac{v_x^d + \frac{B}{2}\omega_z^d}{r_e} \quad (18)$$

The superscript d denotes a desired value. The forward velocity is expressed in meters per second, while the yaw rate and drive angular velocities are expressed in radians per second. The symmetric solution gives the same angular velocity to the front and rear modules on each side.

The extra actuator freedom could be used by a more advanced control algorithm. If the robot can estimate terrain conditions and track loading, it could distribute drive effort differently between the front and rear modules. The same flexibility could also help the robot continue operating after an actuator fault or reduce the effect of slip. These extensions would require additional sensing and a more detailed vehicle-terrain model and are not developed here.

Mobility Assessment

Contact Area and Ground Pressure

To obtain a simple first estimate, each track module is represented by a rectangular contact patch. If all four modules are fully supported, the total nominal contact area is

$$A_{\mathrm{total}} = 4 l_c w_t \quad (19)$$

Here l_c is the nominal contact length of one module and w_t is the track width. Both are measured in meters, so A_{total} is measured in square meters.

For a vehicle of mass m, the corresponding nominal mean ground pressure is

$$p_g = \frac{mg}{A_{\mathrm{total}}} = \frac{mg}{4 l_c w_t} \quad (20)$$

In Eq. (20), g is the gravitational acceleration in meters per second squared and p_g is expressed in pascals. This is only an average value, as the real pressure is not uniform when the ground deforms or the vehicle moves over uneven terrain.

These equations show why longer and wider contact patches can reduce the nominal mean ground pressure, but contact area alone does not determine soft-ground performance. Vehicle mass, terrain stiffness, sinkage, and load transfer still influence whether the robot can move without excessive resistance [4].

Turning

When the two sides move at different speeds, the nominal turning radius measured from the vehicle reference point to the instantaneous center of rotation is

$$R = \frac{B}{2}\frac{v_R + v_L}{v_R - v_L} \quad (21)$$

The radius R and spacing B are measured in meters. If the two side velocities are equal, the denominator becomes zero and the vehicle moves straight rather than along a finite-radius turn.

If the two sides move with equal magnitude in opposite directions, the ideal model gives

$$v_R = -v_L \;\Rightarrow\; R = 0 \quad (22)$$

This is the nominal pivot-turn condition. If both side velocities are zero, the robot is stationary and no turning radius is defined.

A pivot turn is useful in narrow passages and cluttered interiors, but it comes at a cost. The tracks must scrub laterally against the ground, which increases steering resistance

and power loss. Measurements on skid-steered tracked robots show that these losses can be substantial [6].

Obstacle Negotiation

The separated front and rear modules create two contact regions on each side of the vehicle. When the robot approaches a step, one module may reach the upper surface while another still carries load below. This can help on discontinuous ground, but the gap between the modules can also become a disadvantage. What happens depends on the center of mass, the shape of the obstacle, the available traction, and how the load shifts between the modules. Passive suspension follows the terrain without an active command [8,9], while flippers can deliberately change the approach angle and support point [10,11].

Contact area alone therefore does not tell us which architecture will cross an obstacle more easily. A rigid dual-track robot keeps one fixed support envelope, while the four-track layout divides it into front and rear regions. Passive suspension lets the running gear change orientation with the terrain. Flippers go further by adding actively controlled joints. Habibian et al. showed that climbing performance depends not only on the robot geometry, but also on where the center of mass is located and on the shape of the obstacle [11].

Applicability to SAR Operations

For rescue work, a rigid four-track robot is most attractive when the mission calls for tight skid steering, a robust chassis, modular drives, and a stable platform for sensors or payloads. It is a less suitable choice when the robot must climb very high steps or keep continuous contact with strongly irregular terrain. In those cases, passive suspension or articulated flippers may justify their extra mechanical and control complexity. The architecture should therefore be chosen for the expected rescue task rather than for a single mobility measure.

Results and Discussion

The model relates the four drive speeds to two body motions. The sum of the four drive speeds determines the nominal forward velocity, while the difference between the summed right- and left-side speeds determines the yaw rate. The 2x4 Jacobian keeps all four drive inputs explicit while describing the vehicle motion with only two variables.

The equations also show that the lateral spacing B and effective drive radius r_e determine the planar velocity relation. The longitudinal spacing L does not appear in the reduced Jacobian because the front and rear modules contribute symmetrically in this model. However, L still affects how the vehicle is supported on the terrain and how it approaches an obstacle. The reduced model is therefore suitable for basic velocity control, but it cannot describe the full behavior of the vehicle on rough terrain.

Since **J** has rank two and four inputs, the inverse solution is not unique. A rule is therefore needed to divide the commands among the four drives. The Moore–Penrose pseudoinverse gives a symmetric solution in which the front and rear modules on the same side receive the same command. If the modules are allowed to receive different commands, the remaining freedom could be used to change how the drive effort is shared or to keep the robot moving after an actuator fault. This would require additional measurements.

The basic motion cases follow directly from the equations. Equal speeds at all four modules produce straight nominal motion. Unequal left- and right-side speeds in the same direction produce a finite-radius turn. For equal and opposite side speeds, $\omega_R = \omega_S$ $\omega_L = -\omega_S$, the forward speed becomes zero and Eq. (23) gives the ideal pivot-turn yaw rate.

$$\omega_z = \frac{2r_e}{B}\omega_s \qquad (23)$$

Equation (23) gives the ideal yaw rate for this pivot-turn command.

These cases show that the equations give the expected motion, but they do not demonstrate trajectory accuracy on real terrain. Skid steering introduces terrain-dependent slip, and experiments with four-track robots show that online slip estimation improves tracking [7]. The present model should therefore be treated as a nominal basis for control and track-based odometry rather than as a complete description of terrain interaction.

Numerical Evaluation of the Kinematic Model

A numerical simulation was performed to demonstrate how the proposed model maps the four drive commands to the planar motion of the robot. The simulation used B=0.325 m and $r_e = 0.028$ m. The initial pose was x(0)=0, y(0)=0, and θ(0)=0. Each motion case was simulated over a period of 5 s.

The kinematic model was implemented in Python. NumPy was used for the numerical calculations, and the pose equations were integrated using the explicit Euler method with a time step of Δt=0.01 s. At each step, the vehicle pose was updated as:

$$x_{k+1} = x_k + v_x \cos\theta_k \, \Delta t, \quad (24)$$

$$y_{k+1} = y_k + v_x \sin\theta_k \, \Delta t, \quad (25)$$

$$\theta_{k+1} = \theta_k + \omega_z \, \Delta t. \quad (26)$$

The resulting motion was plotted using Matplotlib. The simulation represents the nominal kinematic model and does not include terrain-dependent slip.

The same calculation sequence was used for all three motion cases. First, the angular speed of each drive was converted to nominal belt speed using Eq. (5).

The front and rear modules on each side were then combined using Eqs. (6) and (7) to obtain the equivalent left- and right-side velocities v_L and v_R. These velocities were used in Eqs. (8) and (9) to calculate the longitudinal velocity $v_x$and yaw rate ω_z. Finally, the pose equations were integrated over the simulation interval.

To make the three cases directly comparable, the drive speeds were selected around a common reference angular speed of 10 rad s^{-1}. This value is used only for the numerical comparison and is not tied to a specific motor model. Straight motion uses the same reference speed on both sides. For the constant-radius turn, the mean drive speed remains 10 rad s^{-1}, while a symmetric difference of ±2 rad s^{-1} is applied between the left and right sides, giving $\omega_L = 8\,rad\,s^{-1}$ and $\omega_R = 12\,rad\,s^{-1}$. For the pivot turn, the same speed magnitude is retained but with opposite signs.

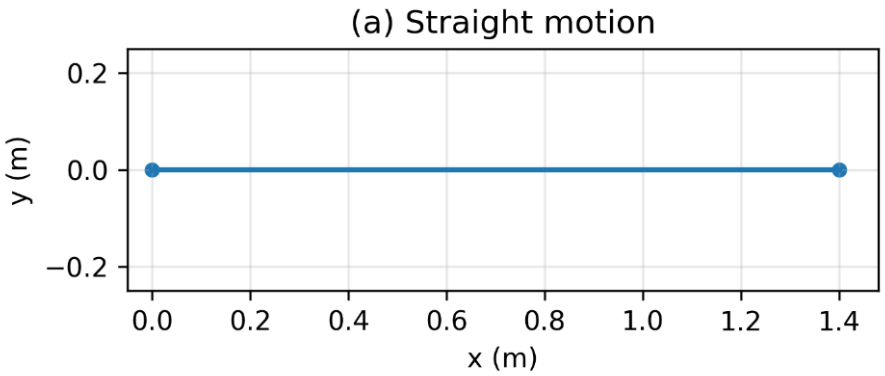
For straight motion, Eqs. (5)-(7) give

$$v_{\mathrm{L}} = v_{\mathrm{R}} = 0.280\ \mathrm{m\,s^{-1}}, \quad (27)$$

and therefore

$$v_x = 0.280\ \mathrm{m\,s^{-1}}, \qquad \omega_z = 0. \quad (28)$$

After 5 s, the simulated position is x=1.40m and $y = 0$.



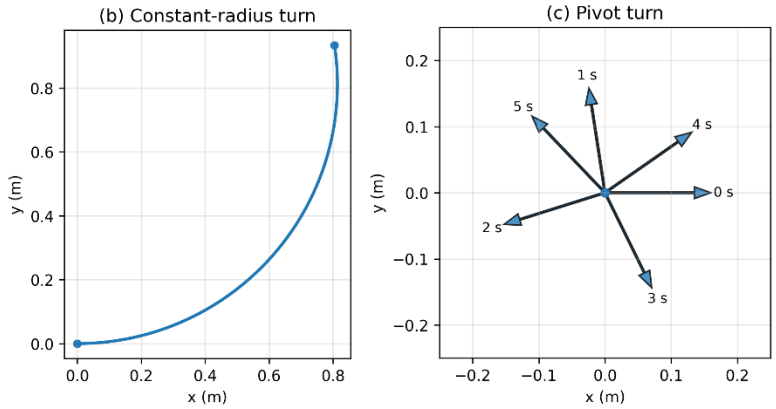


***Fig. 2**. Simulated planar motion for (a) straight motion, (b) constant-radius turn, and (c) pivot turn.*

For the constant-radius turn, the corresponding side velocities are:

$$v_{\mathrm{L}} = 0.224\,\mathrm{m\,s^{-1}}, v_{\mathrm{R}} = 0.336\,\mathrm{m\,s^{-1}} \quad (29)$$

Using these values in Eqs. (8) and (9), the longitudinal velocity and yaw rate are:

$$v_x = 0.280\,\mathrm{m\,s^{-1}}, \quad \omega_z = 0.345\,\mathrm{rad\,s^{-1}}. \quad (30)$$

Equation (21) gives the nominal turning radius:

$$R = 0.813\,\mathrm{m}. \quad (31)$$

After 5s, the simulated pose is approximately

$$x = 0.805\,\mathrm{m},\ y = 0.934\,\mathrm{m},\ \theta = 1.72\,\mathrm{rad}. \quad (32)$$

For the pivot turn, the side velocities become:

$$v_{\mathrm{L}} = -0.280\,\mathrm{m\,s^{-1}}, v_{\mathrm{R}} = 0.280\,\mathrm{m\,s^{-1}}. \quad (33)$$

The longitudinal velocity is therefore zero, while Eq. (23) gives

$$v_x = 0, \quad \omega_z = 1.72\,\mathrm{rad\,s^{-1}}. \quad (34)$$

The vehicle reference point remains at $x = y = 0$, while its orientation changes with time.

Figure 2 shows the three simulated motion cases. Equal left- and right-side speeds produce straight motion, unequal speeds produce a finite-radius turn, and equal speeds with opposite signs produce a pivot turn. In Fig. 2(c), the arrows indicate the vehicle heading at 1 s intervals from $t = 0$ to $t = 5\,\mathrm{s}$. This case represents an ideal kinematic pivot turn. In a real skid-steered vehicle, lateral track slip is required during rotation, so the actual instantaneous center of rotation and yaw rate may differ from the values predicted by the nominal model.

The simulation confirms that the model produces the expected straight, turning, and pivot motions. The calculated results represent ideal planar motion and should not be interpreted as predictions of the actual vehicle motionon on deformable or high-slip terrain.

Model Limitations

The equations describe nominal planar motion rather than the full behavior of the robot on rough terrain. They do not show how the tracks deform the ground or how the motors respond when the load changes. The model also does not describe changes in pitch and roll. Slip during skid steering can cause track-based odometry to drift unless it is estimated or corrected.

In practice, Eqs. (5)-(14) describe the nominal vehicle motion, while Eqs. (15)-(18) provide the corresponding drive commands. Slip and terrain effects must be treated separately, either with a more detailed model or with sensor data.

The model should next be tested on repeatable mobility tasks rather than on isolated obstacle demonstrations. ASTM response-robot test methods include symmetric stepfields and variable hurdles that can reveal traction limits, rollover tendencies, and the effect of chassis or suspension geometry [12,13]. Gravel tests are also useful because loose aggregate promotes slip and may interfere with the running gear [14].

A suitable test setup would record encoder data, IMU measurements, motor

current, and an external pose reference at the same time. These measurements would allow comparison of trajectory error, slip, power consumption, and obstacle-crossing success under the same test conditions.

CONCLUSION

This study developed a generalized kinematic model for rigid four-track skid-steered UGVs without tying the equations to a specific commercial chassis. The model keeps all four drives explicit in a 2x4 Jacobian matrix. When the Moore–Penrose pseudoinverse is used, the front and rear modules on the same side receive the same command. The equations also show that the effective drive radius and the lateral track spacing determine the nominal planar motion, while the front-to-rear spacing mainly affects how the robot is supported and how it approaches obstacles.

The comparison with other tracked robots shows where the four-track layout can be useful in rescue operations. It provides separate drive modules and compact skid steering without the additional joints used by flipper-equipped robots. However, skid steering still causes lateral scrubbing, and the rigid chassis cannot actively change its support geometry. Passive suspension or articulated flippers may therefore be more suitable when the terrain is highly irregular or when the robot must climb difficult stairs and obstacles.

The model can serve as a starting point for control calculations and track-based odometry, but it should not be treated as a complete prediction of motion on rough terrain. Future work should measure slip and power losses, study how the load shifts between the modules, and test representative four-track robots on standardized stepfields, hurdles, and loose terrain. Direct experiments with dual-track, suspended, and articulated robots would then help determine where the rigid four-track layout provides a practical advantage in search-and-rescue tasks.

REFERENCES

[1] Delmerico J, Mintchev S, Giusti A, Gromov B, Melo K, et al. The current state and future outlook of rescue robotics. Journal of Field Robotics. 2019;36(7):1171-1191. https://doi.org/10.1002/rob.21887.

[2] Murphy RR. Disaster Robotics. Cambridge, MA: MIT Press; 2014. ISBN 978-0262027359.

[3] Wang Z, Gu H. A review of locomotion mechanisms of urban search and rescue robot. Industrial Robot. 2007;34(5):400-411. https://doi.org/10.1108/01439910710774403

[4] Wong JY. Theory of Ground Vehicles. 4th ed. Hoboken, NJ: John Wiley & Sons; 2008. ISBN 978-0470170380.

[5] Martínez JL, Mandow A, Morales J, Pedraza S, García-Cerezo A. Approximating kinematics for tracked mobile robots. The International Journal of Robotics Research 2005;24(10):867-878. https://doi.org/10.1177/0278364905058239.

[6] Morales J, Martínez JL, Mandow A, García-Cerezo AJ, Gómez-Gabriel JM, Pedraza S. Power analysis for a skid-steered tracked mobile robot. 2006 IEEE International Conference on Mechatronics (ICM). 2006:420-425. https://doi.org/10.1109/ICMECH.2006.252564.

[7] Ha XV, Ha C, Lee J. Fuzzy vector field orientation feedback control-based slip compensation for trajectory tracking control of a four track wheel skid-steered mobile robot. International Journal of Advanced Robotic Systems. 2013;10:218. https://doi.org/10.5772/56355.

[8] Galati R, Reina G. Terrain awareness using a tracked skid-steering vehicle with passive independent suspensions. Frontiers in Robotics and AI. 2019; 6:46. https://doi.org/10.3389/frobt.2019.00046.

[9] Gao J, Li Y, Jin J, Jia Z, Wei C. Design, analysis and control of tracked mobile robot with passive suspension on rugged terrain. Actuators. 2025;14(8):389. https://doi.org/10.3390/act14080389.

[10] Chen B, Huang K, Pan H, Ren H, Chen X, Xiao J, Wu W, Lu H. Geometry-based flipper motion planning for articulated tracked robots traversing rough terrain in real-time. Journal of Field Robotics. 2023;40(8):2010-2029. https://doi.org/10.1002/rob.22236.

[11] Habibian S, Dadvar M, Peykari B, Hosseini A, Salehzadeh MH, Hosseini AHM, Najafi F. Design and implementation of a maxi-sized mobile robot (Karo) for rescue missions. ROBOMECH Journal. 2021; 8:1. https://doi.org/10.1186/s40648-020-00188-9.

[12] ASTM International. ASTM E2828/E2828M-20: Standard Test Method for Evaluating Response Robot Mobility Using Symmetric Stepfields Terrains. West Conshohocken, PA: ASTM International; 2020.

[13] ASTM International. ASTM E2802/E2802M-21e1: Standard Test Method for Evaluating Response Robot Mobility Using Variable Hurdle Obstacles. West Conshohocken, PA: ASTM International; 2021.

[14] ASTM International. ASTM E2991/E2991M-25: Standard Test Method for Evaluating Response Robot Mobility: Traverse Gravel Terrain. West Conshohocken, PA: ASTM International; 2025.